Received: 19 October 2020 | Revised: 3 December 2020 | Accepted: 7 December 2020

DOI: 10.1002/pol.20200714

ORIGINAL ARTICLE

JOURNAL OF POLYMER SCIENCE WILEY

Mannosylated fluorescent cellulose-based glycopolymers for stable uniform nanoparticles

Shuang Wang[1] | **Philipp Vana**[2] | **Kai Zhang**[1]

[1]Wood Technology and Wood Chemistry, Department Wood Technology and Wood-based Composites, Georg-August-University of Göttingen, Göttingen, Germany

[2]Institute of Physical Chemistry, Georg-August-University of Göttingen, Göttingen, Germany

Correspondence
Kai Zhang, Wood Technology and Wood Chemistry, Department Wood Technology and Wood-based Composites, Georg-August-University of Göttingen, Büsgenweg 4, D-37077, Göttingen, Germany.
Email: kai.zhang@uni-goettingen.de

Funding information
China Scholarship Council, Grant/Award Number: Shuang Wang; Georg-August-Universität Göttingen; Verband der Chemischen Industrie; Fonds der Chemischen Industrie (FCI)

[Correction added on 16 January 2021, after first online publication: Projekt Deal funding statement has been added.]

Abstract

In living organisms, carbohydrate-protein interactions play key roles in physiological and pathological processes, which are amplified by the "glycol-cluster effect." In this work, we synthesized novel fluorescent cellulose derivatives bearing mannose moieties via thiol-ene click reactions by sequentially conjugating hydrophilic mannose-oxyethoxylpropane-thiol (Mann-SH) and fluorescent coumarin-oxyhexyl-thiol (Coum-SH) and rhodamine B-ethyl-thiol (RhB-SH) to cellulose undecenoate with terminal double bonds. The amphiphilic fluorescent cellulose derivatives were converted into nanoparticles (NPs) by dropping into low ionic strength solutions (<0.085 M). Obtained NPs have average sizes between 240 and 554 nm depending on the solution concentrations, exhibiting uniform size distributions (PDI values <0.12). These uniform NPs exhibited excellent dispersion stability even at elevated temperatures. The mannose moieties were accessible to 1,4-benzenediboronic acid (BDBA) in NaOH aqueous solutions. Under irradiation with UV light of 320–400 nm, the fluorescence of NPs increased by the formation of open-ring rhodamine spiroamide, which could be a promising candidate for biomedical application.

KEYWORDS

cellulose derivative, ionic strength, mannose moieties, nanoparticles, thiol-ene click reaction

1 | INTRODUCTION

Carbohydrate-protein interactions participate in numerous biological activities, such as cellular recognition, adhesion, infection of pathogen and cancer cell metastasis.[1,2] The interactions between clustered saccharides and proteins are strong due to the so-called "glycol-cluster effect" or "multivalent effect."[3] Synthetic glycopolymers containing pendant saccharides have been commonly used to mimic biological recognition events, such as biosensing and diagnosis, targeting cells, drug delivery, and gene delivery.[4–8] Generally, glycopolymers carrying saccharide moieties have been prepared via polymerization of glyco-monomers or post-polymerization modification favored by the highly efficient and selective click reactions.[9,10]

Cellulose is the most abundant polysaccharide of β-(1 → 4)-linked anhydroglucose units (AGUs) and widely distributes in plants, algae, and some bacteria.[11] Cellulose derivatives with diverse functional groups can be obtained by regioselectively chemical modifications of three hydroxyl groups presenting in each AGU.[12] Certain cellulose derivatives can formed nanoparticles with high surface/volume ratio via nanoprecipitation also called "Ouzo effect" or "solvent exchange process," which include

dropping and dialysis techniques.[12] In the past decades, bio-nano/microparticles produced from cellulose derivatives have attracted great attentions due to their potential applications in biomedicine field, such as drug delivery, gene transfection and bioimaging.[13–15] However, cellulose derivatives with carbohydrate pendants have been rarely reported, which could be a group of interesting biomaterials due to many superiorities, such as biocompatibility, nontoxicity and specific recognition ability.[16,17]

For medical and biological applications, fluorescent dyes offer a platform to visualize and track molecular interactions during cellular internalization process.[18] Among them, rhodamine and coumarin fluorophores are commonly used due to their excellent and favorable properties, such as high fluorescent quantum yields, biocompatibility, stable fluorescent emission and sharp fluorescence emissions.[18,19] Besides, the florescence of rhodamine can be greatly enhanced via structural change from the non-fluorescent spirocyclic state to fluorescent open-ring state induced by different stimulus, such as UV light, metal ions, and pH.[20,21]

In the present study, we prepared fluorescent glycopolymers by chemical modification of renewable cellulose. At first, three kinds of mercapto-containing compounds were synthesized: hydrophilic mannose-oxyethoxylpropane-thiol (Mann-SH) and fluorescent coumarin-oxyhexyl-thiol (Coum-SH) and rhodamine B-ethyl-thiol (RhB-SH). Then, they were conjugated to cellulose undecenoate with terminal double bonds via sequentially photo- and thermal-initiated thiol-ene click reactions. The final product 11-(mannose-oxyethoxylpropane)(coumarin-oxyhexyl)(rhodamine-ethyl)thiolundecanoate 10-undecenoyl ester of cellulose (CUE-MCR) was well soluble in organic solvents and further converted into NPs. The properties of NPs bearing mannose moieties were investigated regarding their thermal stability, binding with phenylboronic acid and fluorescence sensitivity.

2 | RESULTS AND DISCUSSION

2.1 | Synthesis of fluorescent amphiphilic 11-(mannose-oxyethoxylpropane)(coumarin-oxyhexyl)(rhodamine-ethyl)thiolundecanoate 10-undecenoyl ester of cellulose (CUE-MCR) via thiol-ene click reaction

In this work, "thiol-ene click chemistry" technique as a highly efficient and practical reaction to fabricate multifunctional polymers was used to attach different mercapto-containing compounds to cellulose backbones with terminal double bonds under mild reaction conditions. At first, three mercapto-containing compounds were synthesized via reactions including glycosylation, acetylation, deacetylation and substitution reactions: mannose-oxyethoxylpropane-thiol (Mann-SH), coumarin-oxyhexyl-thiol (Coum-SH) and rhodamine B-ethyl-thiol (RhB-SH) (Scheme 1(a)–(c)). Besides, compound Mann-SH was hydrophilic and compounds Coum-SH and RhB-SH were hydrophobic and fluorescent. At the same time, we prepared cellulose 10-undecenoyl ester (CUE) under homogenous conditions, which was easily dissolved in THF due to the high degree of substitution ($DS_{C=C}$ = 2.6) according to elemental analysis (Scheme 1(d)). Due to the highly hydrophilic property of Mann-SH and UV-sensitive property of Coum-SH and RhB-SH, we used photo-initiated thiol-ene click reaction between Mann-SH and CUE in the mixture solvents of THF and DMAc for 6 h and sequentially used thermal-initiated thiol-ene click reaction by adding Coum-SH and RhB-SH stirring at 70°C for 10 h. After the two-step thiol-ene click reactions, the final fluorescent amphiphilic product 11-(mannose-oxyethoxylpropane)(coumarin-oxyhexyl)(rhodamine-ethyl) thiolundecanoate 10-undecenoyl ester of cellulose (CUE-MCR) was obtained with DS_{Coum} (1.0), $DS_{C=C}$ (0.9), low DS_{Mann} (0.5) and DS_{Rhod} (0.2), according to elemental analysis and ^{1}H NMR spectroscopy (Scheme S1 and Figure 2). The polymer CUE-MCR was well soluble in several organic solvents, such as THF, DCM, DMAc and DMF.

The representative FTIR spectra of CUE and CUE-MCR were displayed in Figure 1(a). Compared to the FTIR spectra of CUE, the peaks of olefin C—H and C═C at 3077, 1639, and 907 cm^{-1} greatly decreased and the stretching vibration peaks of O—H and C═O (ester carbonyl group and enone carbonyl group) at 3483 and 1735 cm^{-1} broadly increased in the FTIR spectra of CUE-MCR. This fact indicates that the double bonds of CUE were partially consumed and three mercapto-containing compounds (Mann-SH, Coum-SH and RhB-SH) were attached to the CUE during the thiol-ene click reaction. Meanwhile, we observed characteristic absorption peaks for aromatic rings at 1610–1510 cm^{-1} (the C═C stretching vibration) and 870–750 cm^{-1} (the aromatic C—H deformation vibration out of plane), and peak at 1386 cm^{-1} (the —CH_3 deformation vibration), indicating the existence of coumarin and rhodamine B structures.[22] In addition, the new peak appeared at 1280 cm^{-1} which was ascribed to the tertiary aromatic amine N-aryl bond of the rhodamine B moieties. The peaks at 1270 and 693 cm^{-1} were attributed to the —CH_2—S—CH_2— bond.[16] In addition, gel permeation chromatography (GPC) was used to measure the molecular weight of CUE-MCR. As shown in Figure 1(b), the CUE-MCR had the number-average molecular weight (M_n) of 6844 g mol^{-1} and a broad molecular weight distribution (PDI = 14.0).

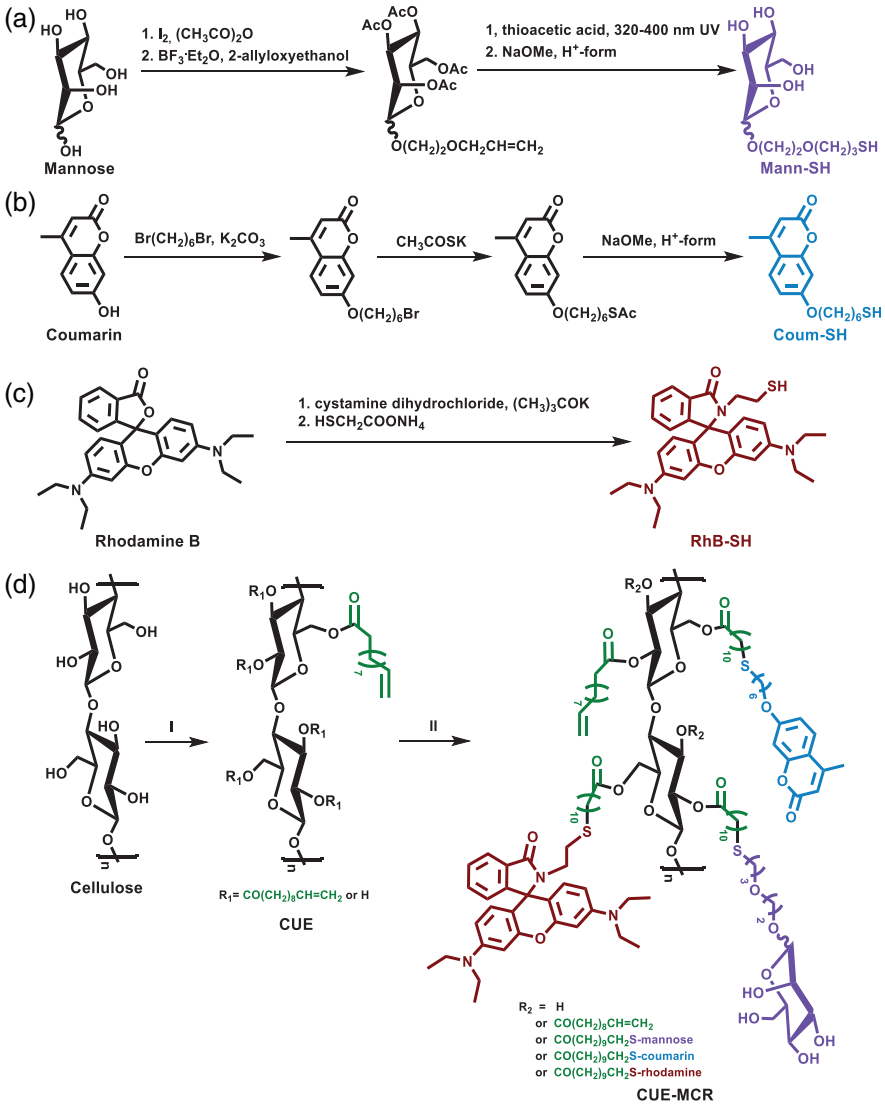

SCHEME 1 Synthetic routes of (a) Mann-SH; (b) Coum-SH; (c) RhB-SH and (d) 11-(mannose-oxyethoxylpropane) (coumarin-oxyhexyl)(rhodamine-ethyl) thiolundecanoate 10-undecenoyl ester of cellulose (CUE-MCR): (i) 10-undecenoyl chloride, pyridine, heating at 50°C for 4 h; (ii) Mann-SH, 320–400 nm UV irradiation for 6 h, DMPA; then Coum-SH, RhB-SH, heating at 70°C for 10 h, AIBN [Color figure can be viewed at wileyonlinelibrary.com]

^{1}H-NMR was employed to further investigate the chemical structure of CUE-MCR, as shown in Figure 2. In the ^{1}H NMR spectrum of CUE, the terminal olefin peaks appeared at 4.9 and 5.8 ppm and the signals from 3.0 to 5.3 ppm can be assigned to the protons of the cellulose backbone, as shown in Figure 2(a). After thiol-ene click reaction, a significant decrease of olefin resonances revealed the most thiol-ene addition. The new peaks at 8.0, 7.5–7.6, 6.8–7.1, 6.1 ppm were assigned to the aromatic and enone protons of rhodamine and coumarin group, respectively. The new signals appeared at 5.4 and 3.3–3.8 ppm and were corresponding to the protons of mannose groups. The presence of these signals confirmed the successful incorporation of mannose, coumarin and rhodamine groups after the two-step thiol-ene click reaction. Moreover, ^{1}H NMR spectrum of CUE-MCR was also used for calculating DS ascribed to functional groups. Since the two-step thiol-ene click reactions were very mild, the double bonds of CUE ($DS_{C=C} = 2.6$) should only be consumed by incorporation of three kinds of functional groups. The integration of typical aromatic peak of rhodamine group at 8.0 ppm, enone peak of coumarin group at 6.1 ppm, the terminal olefin peak at 5.8 ppm and C-1 peak of mannose group at 5.4 ppm yielded a ratio of 0.24:1.00:0.86:0.48, which was in good accordance with the result of elemental analysis.

In addition to the carbon signals assigned to terminal olefin at 114.15 and 138.97 ppm as observed in ^{13}C NMR spectra of CUE, new characteristic signals emerged in the ^{13}C NMR spectra of CUE-MCR assigned to the mannose, coumarin and rhodamine groups (Figure 3). As shown in Figure 3(b), the carbon signals at 61.66, 66.65, 67.89, 69.60, 71.81 and 99.93 ppm were assigned to the mannose ring, while the carbon signals at 18.61, 101.22, 111.71, 112.59, 113.34, 125.42, 152.58, 155.18, 161.30, and 162.08 ppm were attributed to the methyl, cyclic enone and aromatic carbons of coumarin groups, respectively, as displayed in detail in Figure 3(b). The weak carbon signals at 12.54, 50.69, 97.59, 107.99, 124.55, 125.15, 127.96, 128.47, 128.81, 131.40, 148.69, and 153.22 were assigned

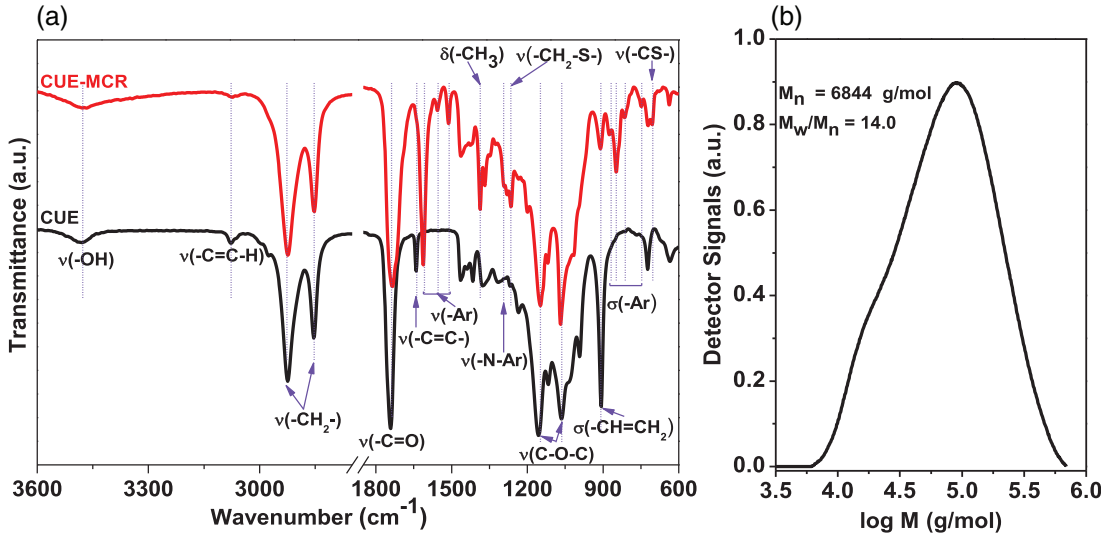

FIGURE 1 (a) FTIR spectra of cellulose 10-undecenoyl ester (CUE) ($DS_{C=C}$ = 2.6) and 11-(mannose-oxyethoxylpropane)(coumarin-oxyhexyl)(rhodamine-ethyl)thiolundecanoate 10-undecenoyl ester of cellulose (CUE-MCR) (DS_{Mann} = 0.5, DS_{Coum} = 1.0, DS_{Rhod} = 0.2 and $DS_{C=C}$ = 0.9). (b) Size exclusion chromatographic curve of CUE-MCR measured in THF [Color figure can be viewed at wileyonlinelibrary.com]

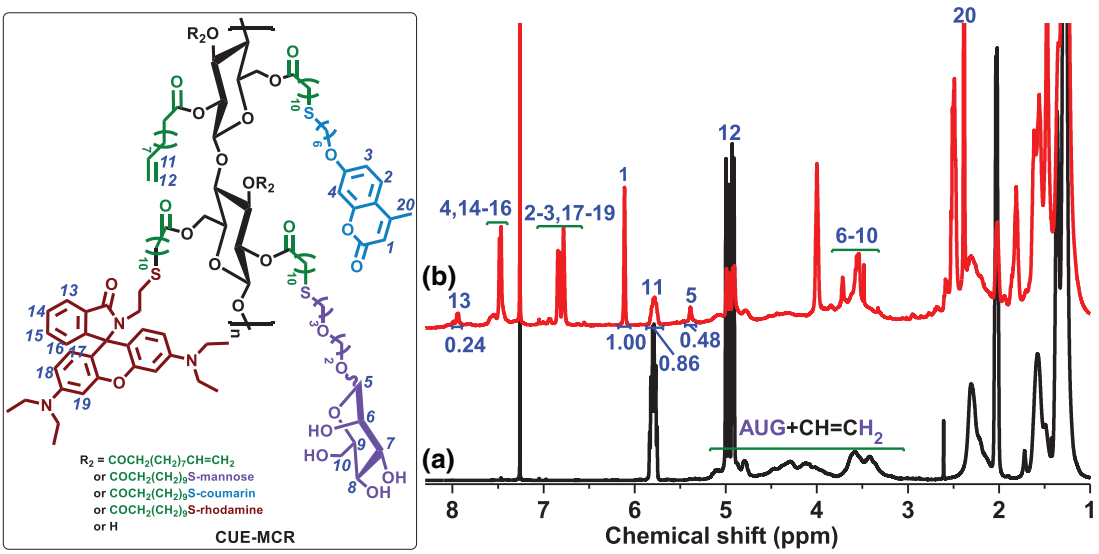

FIGURE 2 ^{1}H NMR spectra of (a) cellulose 10-undecenoyl ester (CUE) ($DS_{C=C}$ = 2.6) and (b) 11-(mannose-oxyethoxylpropane)(coumarin-oxyhexyl)(rhodamine-ethyl)thiolundecanoate 10-undecenoyl ester of cellulose (CUE-MCR) (DS_{Mann} = 0.5, DS_{Coum} = 1.0, DS_{Rhod} = 0.2 and $DS_{C=C}$ = 0.9) measured in $CDCl_3$. The numbers in the structural formula of CUE-MCR display the protons of CUE-MCR [Color figure can be viewed at wileyonlinelibrary.com]

to the methyl and aromatic carbons of rhodamine group due to the low DS.

2.2 | Formation of nanoparticles

The NPs were formed via nanoprecipitation of CUE-MCR using dropping technique through a solvent exchange process (Figure 4(a)). In this work, the ionic strengths of non-solvent affecting average size and size distribution of NPs during nanoparticle formation process was investigated. Three electrolytes were chosen: monovalent salts NH_4Cl, NaCl and divalent salt $MgSO_4$. After dropping CUE-MCR solution in THF with the concentration of 4 mg ml^{-1} into excessive aqueous solutions of electrolytes with various concentrations (0, 17, 51,

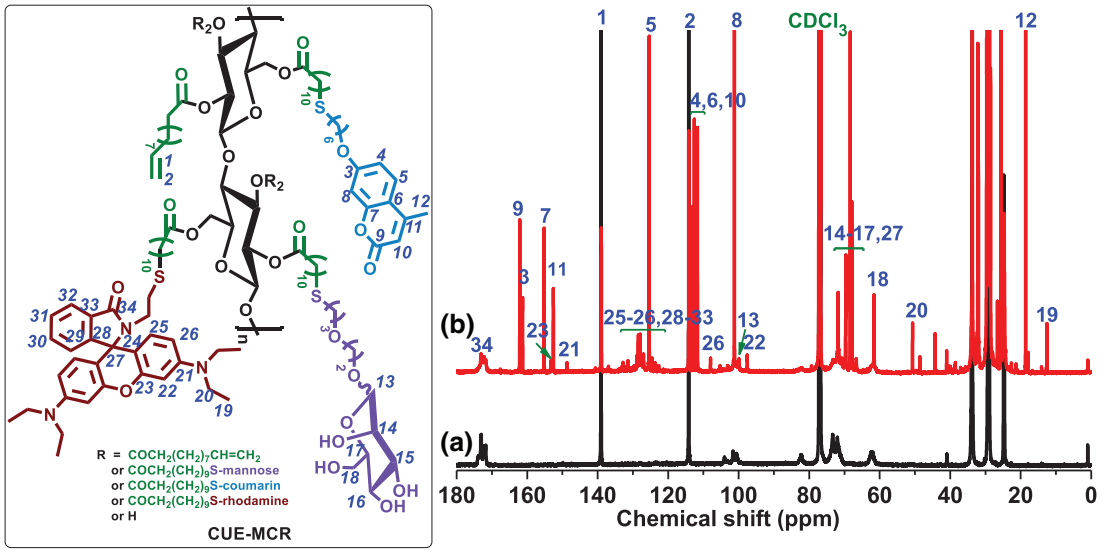

FIGURE 3 ^{13}C NMR spectra of (a) cellulose 10-undecenoyl ester (CUE) ($DS_{C=C} = 2.6$) and (b) 11-(mannose-oxyethoxylpropane)(coumarin-oxyhexyl)(rhodamine-ethyl)thiolundecanoate 10-undecenoyl ester of cellulose (CUE-MCR) ($DS_{Mann} = 0.5$, $DS_{Coum} = 1.0$, $DS_{Rhod} = 0.2$ and $DS_{C=C} = 0.9$) measured in $CDCl_3$ with 15,000 scans. The numbers in the structural formula of CUE-MCR display the carbons of CUE-MCR [Color figure can be viewed at wileyonlinelibrary.com]

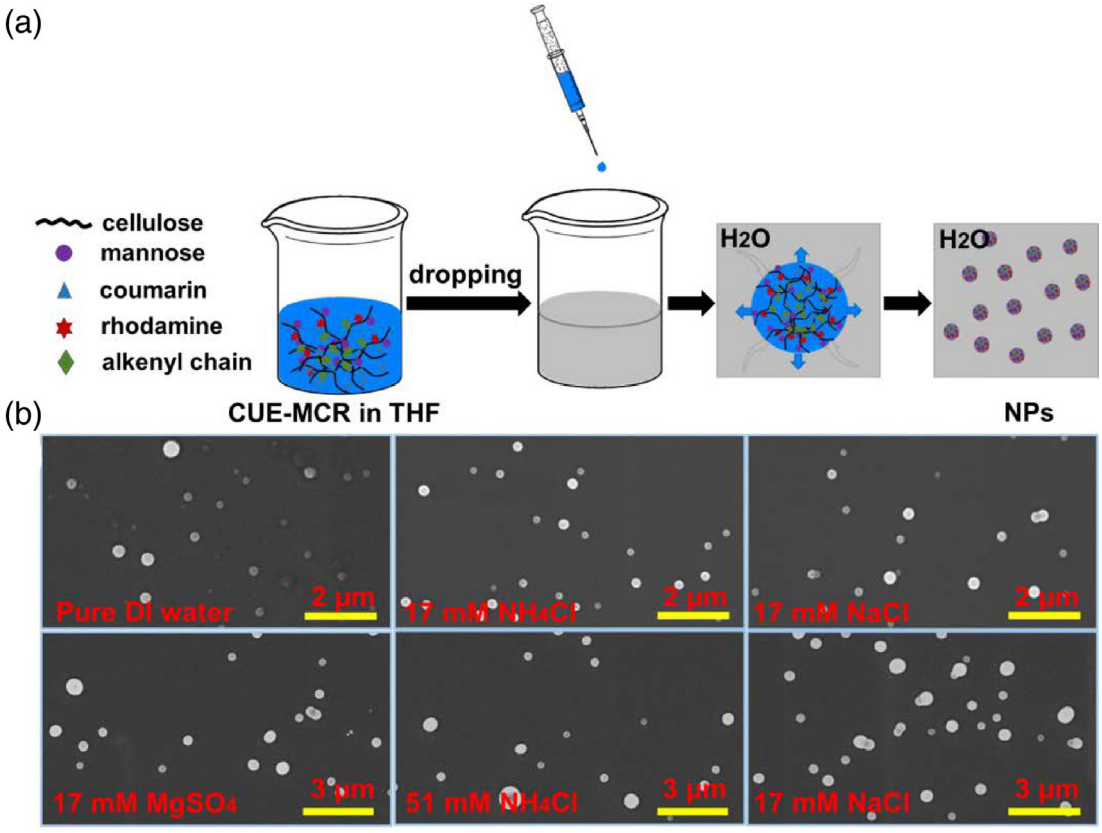

FIGURE 4 (a) Schematic illustration for the nanoprecipitation of CUE-MCR solutions using dropping technique. Blue areas: THF, colorful chains: CUE-MCR chains. (b) SEM images of obtained NPs prepared via dropping into aqueous electrolytes solutions of different concentrations after aging at 80°C for 36 h [Color figure can be viewed at wileyonlinelibrary.com]

85 mM), stable and milky NPs were only obtained in pure DI water and solutions of 17 mM electrolytes (NH_4Cl, NaCl, $MgSO_4$) as well as 51 mM electrolytes (NH_4Cl and NaCl). After the nanoprecipitation, NPs were dialysed against DI water for days to remove THF and electrolytes.

The average size, size distribution and zeta potential were essential parameters for NPs. The average diameters of the resulting NPs ranging from 118 to 560 nm were determined by DLS measurement (Table 1). When using pure DI water as no-solvent (dispersant), the average diameter of NPs was smaller with relatively broader size distribution. In comparison, the presence of electrolytes greatly increased the average sizes of NPs with a more uniform size distribution (PDI value <0.12). At the same lower concentration of electrolytes (17 mM), the average diameters of NPs formed in monovalent electrolyte solutions were smaller than in divalent electrolyte solution. The average diameter of NPs formed in 17 mM $MgSO_4$ was similar to NPs formed in 51 mM NaCl. Using the same electrolyte, the average diameter of NPs increased more than two-fold by increasing the concentration from 17 to 51 mM. The ionic strength of divalent electrolyte $MgSO_4$ was four times higher than an equivalent concentration of monovalent electrolyte NaCl. The presence of low ion valences introduced small electrostatic screening and weakened the electrostatic interactions, leading to the growth of NPs according to nucleation-aggregation mechanism.[23] Thus, stable NPs dispersions in 17 mM solutions of all electrolytes but only in 51 mM solutions of monovalent electrolytes were obtained. The zeta potentials of the stable NPs were between −30.9 and −35.2 mV, confirming the negative surface charges and fairly good physical stability of NPs in these dispersions. With the ionic strength further increased up to 0.085 M, the NPs flocculated instantly upon formation. Therefore, the formation of stable particles is probably strongly limited at higher ionic strengths and/or ion valences (51 mM $MgSO_4$, 85 mM NH_4Cl and 85 mM NaCl), which introduced greater electrostatic screening and strongly reduced surface negative charges.

To investigate the effect of temperature on the dispersion stability of NPs, NPs formed in different electrolytes concentration were incubated at 80°C for 36 h and used DLS to measure the corresponding average diameter and zeta potential of those NPs. After aging for 36 h, NPs with excellent dispersion stability maintained stable and the dispersions stayed transparent. According to their SEM images (Figure 4(b)), spherical NPs of CUE-MCR with a smooth surface remained after aging at 80°C for 36 h. As summarized in Table 1, an increase in temperature resulted in a slight decrease in both the average size and size distribution of those NPs after aging at 80°C compared to initial NPs. The average sizes of those NPs after aging were 225.3 ± 101.7 nm, 260.3 ± 51.0 nm, 253.2 ± 69.0 nm, 473.7 ± 121.1 nm, 477.6 ± 158.2 nm, and 538.4 ± 103.5 nm for NPs formed in pure DI water, 17 mM NH_4Cl, 17 mM NaCl, 17 mM $MgSO_4$, 51 mM NH_4Cl and 51 mM NaCl, respectively. Zeta potential measurements showed that those NPs after aging became more negatively charged. In particular, the zeta potentials of NPs formed in monovalent electrolyte solutions were similar (with the increase of 15–17 mV to around 50 mV) and more than NPs formed in pure DI water or divalent electrolyte solutions (with the increase of 9–10 mV to around 40 mV).

2.3 | Interaction of NPs bearing mannose moieties with BDBA

The NPs bearing monosaccharide units have potential bio-medical applications via protein-clustered saccharides interactions. Besides, boronic acids are considered as synthetic lectins, which are extensively exploited to covalently bind to 1,2- or 1,3-diols of carbohydrates in

TABLE 1 Z-average diameters (d), PDI and zeta potential of NPs formed in aqueous electrolytes solutions of different concentrations using the CUE-MCR solution of 4 mg ml^{-1} THF

Dispersant	Ionic strength (M)[a]	*d* of as-prepared NPs (nm)	PDI	Zeta potential (mV)	*d* of NPs at 80°C for 36 h (nm)	PDI	Zeta potential (mV)
DI water	0	117.8 ± 1.0	0.29 ± 0.04	−31.9 ± 0.4	109.8 ± 5.4	0.26 ± 0.01	−41.2 ± 0.6
NH_4Cl (17 mM)	0.017	239.3 ± 1.2	0.10 ± 0.01	−33.1 ± 0.9	221.9 ± 1.2	0.10 ± 0.02	−48.9 ± 0.6
NaCl (17 mM)	0.017	196.2 ± 0.6	0.08 ± 0.04	−35.0 ± 0.5	187.8 ± 4.1	0.06 ± 0.02	−50.6 ± 0.8
$MgSO_4$ (17 mM)	0.068	471.4 ± 4.7	0.05 ± 0.01	−30.9 ± 0.1	443.0 ± 2.4	0.05 ± 0.02	−39.4 ± 0.4
NH_4Cl (51 mM)	0.051	553.7 ± 7.6	0.12 ± 0.01	−35.2 ± 0.2	477.5 ± 9.1	0.08 ± 0.04	−53.3 ± 0.8
NaCl (51 mM)	0.051	491.0 ± 4.4	0.10 ± 0.02	−34.6 ± 0.6	458.5 ± 0.3	0.02 ± 0.02	−49.5 ± 1.1

[a]The data calculated according the Reference 23.

nonaqueous or alkaline aqueous media.[24,25] The accessibility of pendant mannose moieties on NPs of CUE-MCR was further verified via the interaction of the NPs with BDBA in alkaline aqueous solutions.

Interestingly, the NPs mixing with excess BDBA alkaline solution had good dispersion stability over a period of 100 h. The average diameter of NPs after the incubation with BDBA was determined by DLS measurement. After the incubation for 5, 25, 50, 100 h, the average diameter of NPs formed in 17 mM NH_4Cl remained 246.6 ± 5.7 nm with narrow size distribution (PDI = 0.11 ± 0.02) (Figure 5 (a)), which slightly increased compared to initial NPs with the average size 221.9 ± 1.2 nm and narrow size distribution (PDI = 0.10 ± 0.02). As shown in Figure 5(b), the average diameter of NPs formed in 17 mM MgSO4 remained 500.1 ± 12.5 nm with narrow size distribution (PDI = 0.08 ± 0.03) after the incubation for 5, 25, 50, 100 h. These sizes also slightly increased compared to initial NPs with the average size 443.0 ± 2.4 nm and narrow size distribution (PDI = 0.05 ± 0.02). The results supported the covalent bond between NPs bearing mannose moieties and BDBA under alkaline condition, forming boronic acid-cis diol complexes with strong boronate ester bonds.

NPs together with excess BDBA in alkaline solutions of NaOH were incubated at 60°C (Figure 5(c), sample A). As comparison, NPs in alkaline solution without BDBA (sample B) and alkaline solutions of BDBA without NPs (sample C) were also incubated at 60°C. As shown in Figure 5(c), the NaOH-induced aggregation of NPs was observed in sample B: NPs formed in 17 mM $MgSO_4$ precipitated within 1 h, which significantly faster than the sedimentation of NPs formed in 17 mM NH_4Cl (about 6 h). The reason was that larger average size nanoparticles were more unstable than smaller particles, due to the greater electrostatic screening introduced by NaOH (usually used

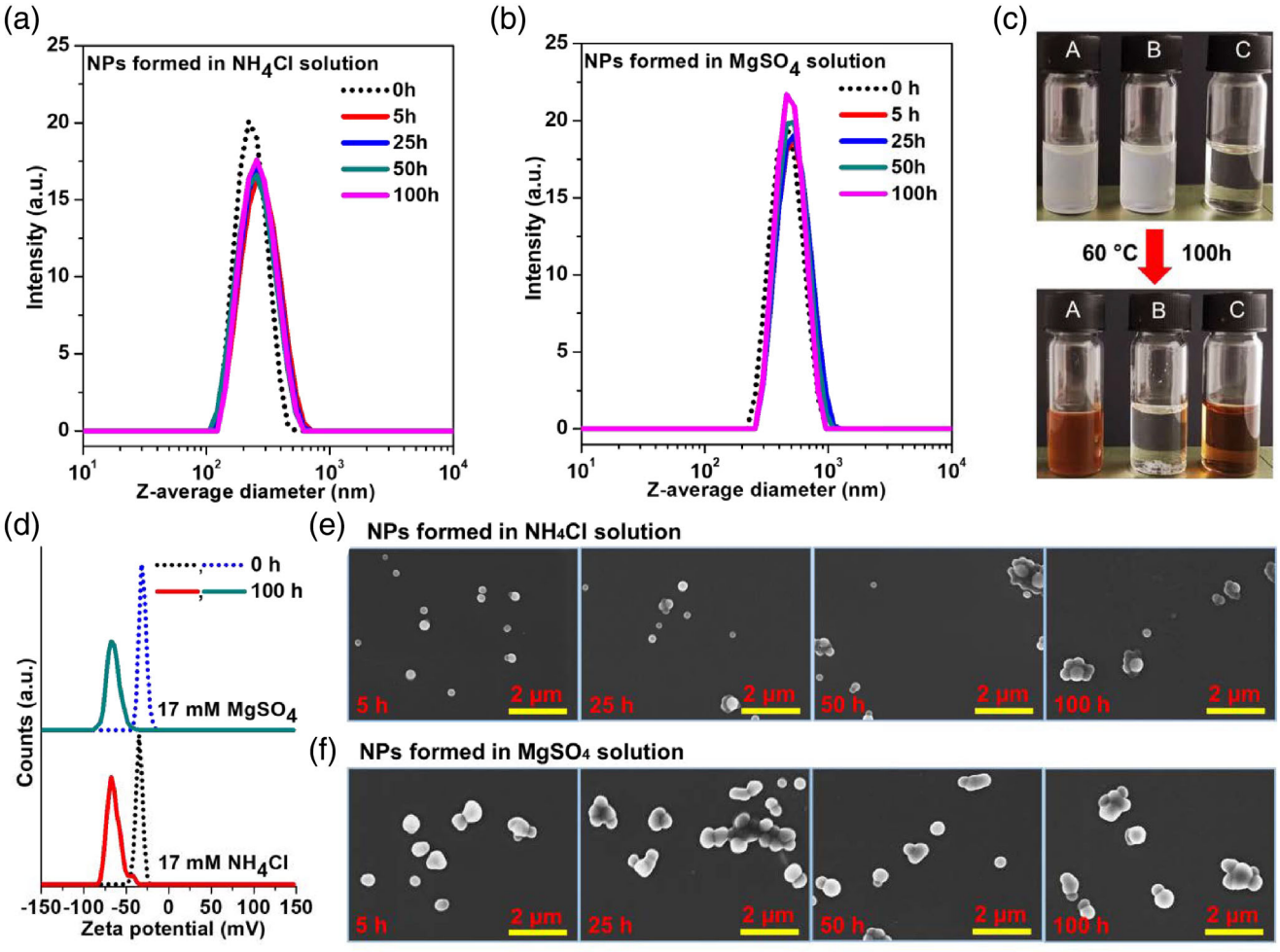

FIGURE 5 DLS curves and SEM images of NPs after incubation in excess BDBA alkaline solution at 60°C for 5, 25, 50, and 100 h: (a) and (e) NPs formed in 17 mM NH_4Cl; (b) and (f) NPs formed in 17 mM $MgSO_4$. (c) Photo image after incubation in NaOH solution at 60°C for 100 h: Sample a containing NPs with excess BDBA, sample B containing NPs without BDBA, and sample C containing BDBA without NPs. (d) Zeta potential curves of NPs after incubation [Color figure can be viewed at wileyonlinelibrary.com]

as precipitation agent). Over the 100 h, the color of sample A changed from milky to yellow and finally to reddish brown, also indicating the formation of tetrahedral boronate anions under alkaline aqueous condition, which was similar to the result observed in sample C only containing BDBA alkaline solution.[26] The tetrahedral boronate anions multivalently bond with clustered mannoses existing on the surface of NPs, transforming nonionic NPs into anionic NPs. The negatively charged NPs had great electrostatic repulsion which can stabilize the NPs against electrostatic screening introduced by NaOH. The slight increases of the average diameter of NPs were caused by the slight aggregation due to electrostatic screening introduced by NaOH. As shown in Figure 5(d), compared with initial NPs, the zeta potentials of NPs in sample A were both greatly increased: the zeta potential of NPs formed in 17 mM NH_4Cl increased from −33.1 to −63.1 mV, and the zeta potential of NPs formed in 17 mM $MgSO_4$ increased from −30.9 to −66.6 mV. Similar results can be obtained when incubated at room temperature over longer time. In addition, the elevated temperature was not necessary but accelerated the resulting aggregateion or binding behavior.

SEM images of NPs incubating with BDBA at 60°C under alkaline condition were shown in Figure 5(e),(f). After the incubation with BDBA in NaOH solution, the spherical morphology of mono-dispersion NPs maintained but those NPs had enhanced tendency to agglomerate over incubation time when dried.

2.4 | Fluorescent properties of NPs

When NPs of CUE-MCR containing coumarin and rhodamine moieties was irradiated with UV light of 320–400 nm for 90 min, a significant decrease of the peak at 328 nm in the UV-Vis spectrum due to the dimerization of the coumarins. As well, there was an increase in the fluorescence

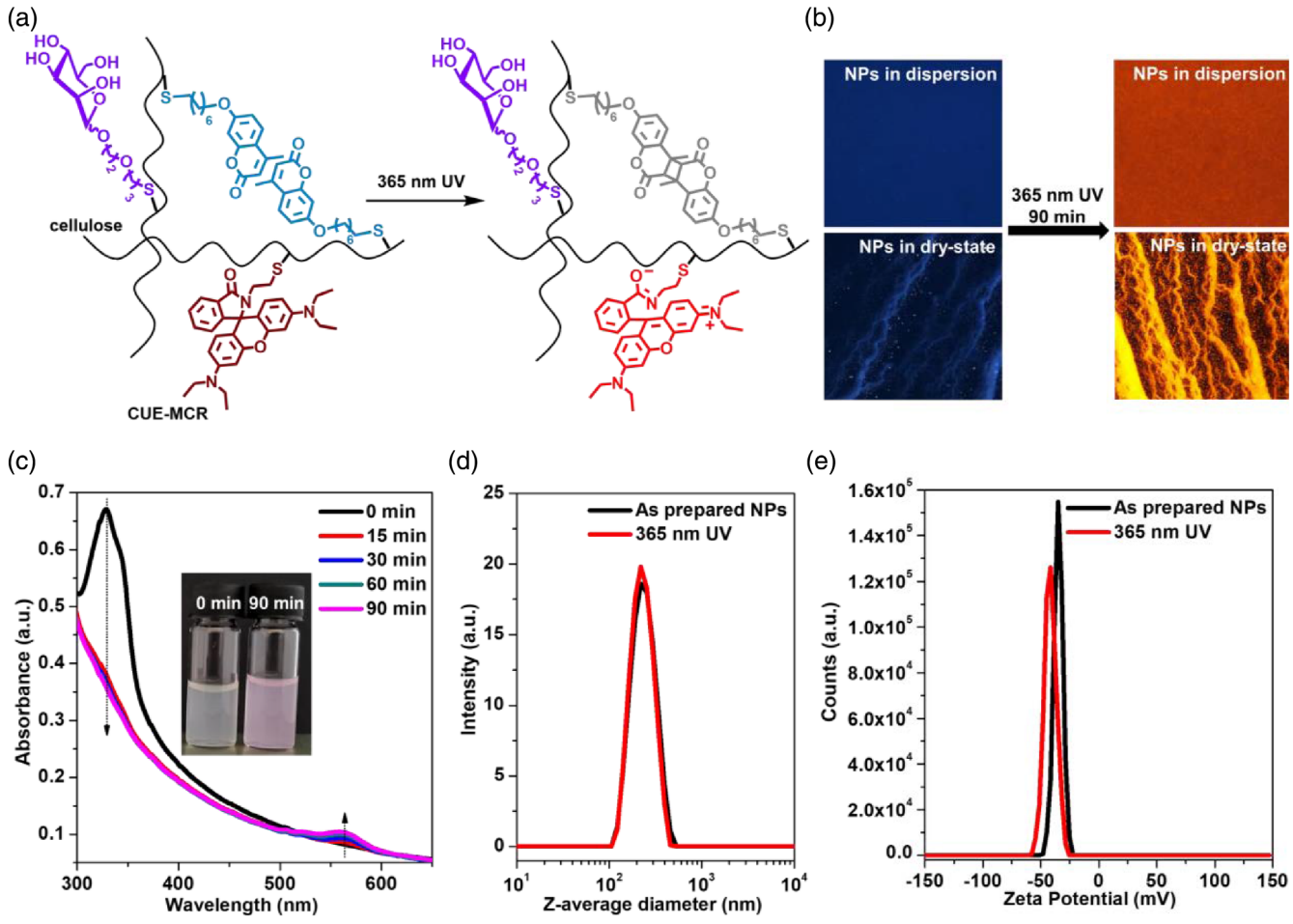

FIGURE 6 UV (365 nm) irradiation of NPs formed in 17 mM NH_4Cl solution for 90 min: (a) dimerization of coumarin and structure change of rhodamine; (b) fluorescent microscopy images of NPs in dispersion and in dry-state; (c) UV–vis spectra, the inset showing the corresponding photographs before and after treatments. (d) DLS curves of NPs before and after treatments. (e) Zeta potential curves of NPs before and after treatments [Color figure can be viewed at wileyonlinelibrary.com]

intensity at 556 nm due to the formation of ring-opened structure of rhodamine from the corresponding non-fluorescent spirolactam structure (Figure 6(a),(c)). Moreover, the strong fluorescence of NPs in dispersion and dry-state was observed by fluorescent microscopy after the irradiation with UV light of 320–400 nm, compared with as-prepared NPs (Figure 6(b)). However, the exposure to 320–400 nm UV light was not sufficient enough to change the average diameter of NPs significantly, but changed zeta potential of NPs. The average diameter of NPs determined by DLS measurement decreased from 239 ± 1 to 218 ± 1 nm after the irradiation with UV light of 320–400 nm for 90 min (Figure 6(d)). PDI greatly decreased simultaneously from 0.208 ± 0.014 to 0.083 ± 0.013, while the zeta potential value obviously increased from -33.1 ± 0.9 to -41.2 ± 0.8 mV, as shown in Figure 6(e). By irradiating the NPs solution with 254 nm UV light for 90 min, an obvious peak increase at 328 nm in the UV–Vis spectrum due to the cleavage of coumarin dimer is notable. At the same time, the fluorescence intensity at 556 nm decreased due to the degradation of rhodamine under irradiation with UV light of 254 nm (Figure S1).

The results showed that NPs of CUE-MCR was highly UV sensitive, which greatly enhanced the fluorescence of NPs by forming open-ring rhodamines. Besides, the coumarin moieties of NPs were photo-switchable, with accompanying fluorescence and stabilizing NPs by dimerization.

3 | CONCLUSION

In summary, we obtained uniform NPs of novel fluorescent cellulose derivatives bearing mannose moieties and coumarin as well as rhodamine moieties. The preparation of final product CUE-MCR started from esterification of cellulose to obtain cellulose backbone with terminal double bonds (CUE) and then two-step thiol-ene click reaction between three mercapto-compounds and CUE. The CUE-MCR with $DS_{Mann} = 0.5$, $DS_{Coum} = 1.0$, $DS_{Rhod} = 0.2$ and $DS_{C=C} = 0.9$ was soluble in organic solvents, such as THF, and were converted into stable NPs via nanoprecipitation. When dropping CUE-MCR solution into aqueous solutions with low ionic strengths (<0.085 M), the average sizes of NPs with uniform size distribution (PDI < 0.12) increased along with ionic strength. The NPs were thermal stable due to the sufficiently high zeta potential. Furthermore, obtained NPs bearing mannose moieties can multivalently bind with BDBA in alkaline solution, stabilizing dispersions in NaOH solution even at elevated temperatures. Irradiation with UV light of 320–400 nm increased the fluorescence of the NPs bearing mannose moieties, which had potential application in biomedical fields.

4 | EXPERIMENTAL

4.1 | Materials and Methods

Microcrystalline cellulose (MCC) with the average size of 50 μm was received from Sigma-Aldrich (Steinheim, Germany). 10-Undecenoyl chloride, pyridine, lithium chloride, D-Mannose, boron trifluoride-ethyl etherate ($BF_3{\cdot}Et_2O$), iodine, sodium methoxide, 2-allyloxyethanol, thioacetic acid, 7-hydroxy-4-methylcoumarin, 1,6-dibromohexane, potassium thioacetate, ion exchange resin (H^+-form), rhodamine B, cystamine dihydrochloride, potassium tert-butoxide, ammonium thioglycolate solution, 2,2-dimethoxy-2-phenylacetophenone (DMPA) and organic solvents including dichloromethane (DCM), ethyl acetate (EtOAc) and *n*-hexane were bought from Th. Geyer GmbH (Germany). Azobisisobutyronitrile (AIBN) was bought from TCI (Japan). Deionized water (DI water) was purified on a Merck Millipore system.

4.1.1 | Synthesis of mannose-oxyethoxylpropane-thiol (Mann-SH)

Mann-SH was synthesized from commercially available D-mannose in three steps according to previous report with a few modifications.[27,28] First step: iodine (0.2 g) was added to a stirred mixture of acetic anhydride (30 ml) and D-mannose (5.0 g, 27.8 mmol). the reaction mixture was allowed to stir at room temperature until the solid was completely dissolved. Then, saturated Na_2SO_3 aqueous solution (10 ml) and saturated $NaHCO_3$ aqueous solution (50 ml) were added sequentially. The mixture was then diluted with DCM (100 ml) and washed against brine solution. After the solvent was removed under reduced pressure, a yellow oily product **1** was obtained without further purification. Second step: a solution of compound 1 (1.0 g, 2.5 mmol) and 2-allyloxyethanol (0.4 ml, 3.3 mmol) in DCM (30 ml) was kept in ice-bath for 10 min under nitrogen protection. Then, $BF_3{\cdot}Et_2O$ (0.4 ml, 3.3 mmol) was added dropwise. The mixture was allowed to stir in ice-bath for another 10 min and then at ambient temperature for overnight. The solution was added into ice water, extracted with DCM and washed with saturated $NaHCO_3$ aqueous solution. The crude product was purified using silica gel column chromatography (*n*-hexane/EtOAc = 4:1) and gave yellow oily product **2**. Third step: A solution of compound **2** (1.0 g, 2.3 mmol) and thioacetic acid (3.3 ml, 46.0 mmol) in DCM solution was stirred under UV irradiation for 2 days. After the extra thioacetic acid was removed by evaporation, sodium methoxide was added slowly until the pH was 10 by pH test paper. The mixture was stirred

overnight at room temperature. Thereafter, ion exchange resin (H^+-form) was added to adjust the pH to neutral. The crude product was purification by silica gel column chromatography (EtOAc/methanol = 1:4) to afford a red oily product **3**. Yield: 24%.

4.1.2 | Synthesis of coumarin-oxyhexyl-thiol (Coum-SH)

Coum-SH was synthesized from commercially available 7-hydroxy-4-methylcoumarin in 3 steps according to previous report with a few modifications.[29] First step: anhydrous K_2CO_3 (0.8 g, 5.7 mmol) and 1,6-dibromohexane (1.8 ml, 11.4 mmol) were added to a solution of 7-hydroxy-4-methylcoumarin (0.5 g, 2.8 mmol) in acetone (5 ml), and the mixture was refluxed for 10 h. After cooling down to room temperature, the reaction mixture was filtered and the filtrate was evaporated under reduced pressure. The crude product was purified on silica gel chromatography (*n*-hexane/EtOAc = 4:1) to afford white solid compound **4**. Second step: potassium thioacetate (0.5 g, 4.5 mmol) was added to a solution of compound **4** (1.0 g, 3 mmol) in DMF (5 ml). The mixture was stirred at room temperature for overnight. When finished, the mixture was poured to water and extracted with ethyl acetate. The solvent was removed by rotary evaporation and the crude product was purified on silica gel chromatography (*n*-hexane/EtOAc = 4:1) to afford white solid compound **5**. Third step: sodium methoxide was added slowly to a solution of compound **5** in methanol until the pH was 10 by pH test paper. The mixture was stirred overnight at room temperature. Then, ion exchange resin (H^+-form) was added to adjust the pH to neutral. The crude product was purification by silica gel column chromatography (*n*-hexane/EtOAc = 4:1) to afford white solid compound **6**. Yield 50%.

4.1.3 | Synthesis of rhodamine B-ethyl-thiol (RhB-SH)

RhB-SH was synthesized according to the literature with a few modifications.[30] Under argon gas protection, cystamine dihydrochloride (5.2 g, 33.8 mmol), potassium tert-butoxide (4.5 g, 40.0 mmol) and rhodamine B (1.2 g, 2.6 mmol) were dispersed in ethanol and refluxed for 24 h. The solvent was removed by evaporation thereafter. Then, 10 ml ammonium thioglycolate aqueous solution (60%) was added to the solution of crude product in DCM (20 ml). The mixture was stirred for overnight at room temperature. After that, the reaction mixture was extracted with DCM (100 ml) and washed against water for three times and the organic solvent was removed by evaporation and purified by silica gel column chromatography (*n*-hexane/EtOAc = 4:1) to yield yellow solid compound **7**. Yield: 40%.

4.1.4 | Synthesis of polymeric cellulose 10-undecenoyl ester (CUE) under homogeneous condition

CUE was synthesized homogenously according to the previous report with a few modifications.[31] MCC was dried at 80°C for 12 h and lithium chloride was dried at 130°C for 2 h under the vacuum of less than 133 Pa before use. 1.0 g MCC was suspended in 40 ml DMAc and the mixture was kept at 130°C for 2 h under rigorous stirring. After removing the oil-bath and cooling down to 100°C, 2 g lithium chloride was added. The mixture was stirred for overnight until a clear solution was obtained. Then, the cellulose solution was heated up to 50°C and 4.1 ml of 10-undecenoyl chloride (3 mol 10-undecenoyl chloride per mol anhydroglucose units in cellulose) was added. Thereafter, 4.9 ml pyridine was added under stirring. The mixture was then stirred for additional 4 h at 50°C and stopped by pouring the warm mixture into five volumes of methanol. Thereafter, the product was separated via centrifugation and purified by repeated dissolution in THF and precipitation in methanol. Yield: ~3.0 g CUE. Degree of substitution ascribed to double bonds $DS_{C=C}$ is 2.6 according to elemental analysis: C 69.03%, H 9.64%.

4.1.5 | Synthesis of 11-(mannose-oxyethoxylpropane)(coumarin-oxyhexyl)(rhodamine-ethyl)thiolundecanoate 10-undecenoyl ester of cellulose (CUE-MCR) via thiol-ene click reaction

0.7 g CUE was dissolved in 70 ml THF at room temperature and the solution of 1.9 g Mann-SH (2 mol per mol C═C double bonds) and 0.5 g DMPA in 20 ml DMAc were added. Under argon protection, the mixture was stirred under UV irradiation (320–400 nm with the intensity of ~100 $mW \cdot cm^{-2}$) for 6 h. Then 4.6 g Coum-SH (5 mol per C═C double bonds), 0.9 g RhB-SH (0.6 mol per C=C double bonds) and 1.5 g AIBN were added to the mixture solution and was stirred at 70°C for 10 h. The mixture was condensed by removing THF and poured into 5 volumes of methanol. The product was separated via centrifugation and purified by repeated dissolution in THF and precipitation in methanol. Yield: ~ 0.9 g CUE-MCR. Degrees of substitutions ascribed

to mannose groups (DS_{Mann}), coumarin groups (DS_{Coum}), rhodamine groups (DS_{Rhod}) and double bonds ($DS_{C=C}$) are 0.5, 1.0, 0.2, and 0.9, respectively, according to elemental analysis and ^{1}H NMR spectra. Elemental analysis: C 66.90%, H 8.6%, N 0.78%, S 4.85%.

4.1.6 | Fabrication of NPs from CUE-MCR

CUE-MCR was converted into NPs via nanoprecipitation using dropping technique. CUE-MCR was dissolved in THF at a concentration of 4 mg ml^{-1}. Then, 1 ml CUE-MCR solution was added dropwise to 10 ml DI water or various electrolyte solutions of different concentrations (17, 51, and 85 mM of NH_4Cl/NaCl/$MgSO_4$) under a stirring of 600 rpm at room temperature. After the complete addition, the samples were subsequently dialysed (molecular weight cut-off 3500) against DI water for 2 days to remove THF and electrolytes before further characterization.

4.1.7 | Incubation NPs solution with BDBA in alkaline condition at 60°C

BDBA alkaline solution was prepared by dissolving 30 mg of BDBA in 1 ml NaOH solution (containing 10 mg NaOH) under sonication. Sample A: 1 ml NPs (formed in 17 mM NH_4Cl/$MgSO_4$ solution and subsequently dialysed in DI water) was added to 1 ml BDBA alkaline solution and then incubated at 60°C in oven for different periods of time. Sample B: 1 ml NPs (formed in 17 mM NH_4Cl/$MgSO_4$ solution and subsequently dialysed in DI water) was added to 1 ml NaOH solution (containing 10 mg NaOH) and then incubated at 60°C in oven for different periods of time. Sample C: 1 ml DI water was added to 1 ml BDBA alkaline solution and then incubated at 60°C in oven for different periods of time.

4.2 | Characterization

4.2.1 | Elemental analysis

The contents of carbon, hydrogen, nitrogen and sulfur were determined with an Elemental Analyzer 4.1 vario EL III (Elementar, Germany).

4.2.2 | FTIR spectroscopy

FTIR spectroscopy was conducted on Bruker Alpha FTIR Spectrometer (Bruker, Germany) at room temperature. All polymer samples were measured between 4000 and 400 cm^{-1} with a resolution of 4 cm^{-1} using Platinum ATR and accumulated 24 scans.

4.2.3 | Liquid-state ^{1}H and ^{13}C NMR spectra

All polymer samples in $CDCl_3$ were obtained at 25°C on Bruker DRX 500 spectrometer (Bruker, Biospin GmbH, Ettlingen). For ^{1}H NMR spectra, scans of up to 16 were accumulated with a frequency of 500.3 MHz. For ^{13}C NMR spectra, scans of up to 15,000 were accumulated with a frequency of 125.8 MHz. Liquid-state NMR spectra were performed at 300 MHz (^{1}H-NMR) and 75 MHz (^{13}C-NMR, APT) on Bruker Avance III 300 and Avance III 400 instruments in the solvent indicated. Chemical shifts (δ) were given in ppm and referenced to the residual solvent signal of $CDCl_3$.

4.2.4 | Scanning electron microscopy (SEM)

SEM images were obtained on a LEO supra-35 high-resolution field emission scanning electron microscope (Carl Zeiss AG, Germany) with an electron beam acceleration voltage of 5 kV. A layer of carbon was coated on the surface of samples before SEM measurements.

4.2.5 | Size exclusion chromatography (SEC)

SEC characterization of CUE-MCR was measured with THF as the eluent on an Agilent 1260 Infinity system consisting of an autosampler (Agilent 1260 Infinity Standard Autosampler), an isocratic solvent pump (Agilent 1260 Infinity), a precolumn of the type SDV (8 mm × 50 mm, particle size 10 μm) from the company Polymer Standard Services (PSS), three separation columns of the type SDV (8 mm × 300 mm, nominal particle size 10 μm, with pore sizes of 10^6, 10^5, and 10^3 Å) from PSS maintained at 35°C in a column compartment and a refractive index detector. An injection volume of 50 μl of CUE-MCR solution in THF at the concentration of 1 g L^{-1} was measured and the flow rate of the mobile phase was 1 ml min^{-1}. Sample CUE-MCR was filter with the pore size of 0.45 μm before the injection.

4.2.6 | Dynamic light scattering (DLS)

DLS measurements were performed on a Zetasizer Nano ZS (Malvern Instruments Ltd., UK) using 5 mW laser with the incident beam of 633 nm (He–Ne laser). 1.2 ml

of NPs suspensions (4 mg ml^{-1} different aqueous solutions) were used for the size measurement (Z-average diameter) in a disposable cuvette (IDL GmbH, Gießen, Germany), and were used for zeta potential measurement in disposable zeta cuvette (DTS1060C from Malvern Instruments Ltd.). The sizes and zeta potentials (mV) of NPs were measured three times with 15 and 20 runs for each measurement, respectively.

ACKNOWLEDGMENTS

Kai Zhang thanks Georg-August-University of Goettingen for the Department Start-up funding and Fonds der Chemischen Industrie (FCI) for the financial support. Shuang Wang gratefully acknowledges her PhD scholarship from the Chinese Scholarship Council (CSC). Open access funding enabled and organized by Projekt DEAL.

CONFLICT OF INTEREST

The authors declare no conflict of interest.

ORCID

Shuang Wang https://orcid.org/0000-0003-2610-4169
Kai Zhang https://orcid.org/0000-0002-5783-946X

REFERENCES

[1] I. Goldstein, R. Iyer, E. Smith, L. So, *Biochemistry* **1967**, *6*, 2373.
[2] H. Lis, N. Sharon, *Chem. Rev.* **1998**, *98*, 637.
[3] Y. C. Lee, R. T. Lee, *Acc. Chem. Res.* **1995**, *28*, 321.
[4] S. S. Ting, G. Chen, M. H. Stenzel, *Polym. Chem.* **2010**, *1*, 1392.
[5] Y. Miura, Y. Hoshino, H. Seto, *Chem. Rev.* **2016**, *116*, 1673.
[6] J. S. Basuki, L. Esser, H. T. Duong, Q. Zhang, P. Wilson, M. R. Whittaker, D. M. Haddleton, C. Boyer, T. P. Davis, *Chem. Sci.* **2014**, *5*, 715.
[7] F. Suriano, R. Pratt, J. P. Tan, N. Wiradharma, A. Nelson, Y.-Y. Yang, P. Dubois, J. L. Hedrick, *Biomaterials* **2010**, *31*, 2637.
[8] R. Jelinek, S. Kolusheva, *Chem. Rev.* **2004**, *104*, 5987.
[9] M. Okada, *Prog. Polym. Sci.* **2001**, *26*, 67.
[10] S. G. Spain, M. I. Gibson, N. R. Cameron, *J. Polym. Sci. Polym. Chem.* **2007**, *45*, 2059.
[11] Y. Habibi, L. A. Lucia, O. J. Rojas, *Chem. Rev.* **2010**, *110*, 3479.
[12] Y. Wang, T. Heinze, K. Zhang, *Nanoscale* **2016**, *8*, 648.
[13] F. Fayazpour, B. Lucas, C. Alvarez-Lorenzo, N. N. Sanders, J. Demeester, S. C. De Smedt, *Biomacromolecules* **2006**, *7*, 2856.
[14] S. Dong, M. Roman, *J. Am. Chem. Soc.* **2007**, *129*, 13810.
[15] E. Bulut, O. Şanlı, *Artif. Cells Nanomed. Biotechnol.* **2016**, *44*, 431.
[16] S. Wang, K. Zhang, *Carbohydr. Polym.* **2018**, *196*, 154.
[17] K. Yoshida, M. Kaino, M. Sekiguchi, N. Chigira, Y. Amano, M. Inokuchi, Q. Li, T. Hasegawa, *Carbohydr. Polym.* **2019**, *223*, 115062.
[18] M. Sakabe, D. Asanuma, M. Kamiya, R. J. Iwatate, K. Hanaoka, T. Terai, T. Nagano, Y. Urano, *J. Am. Chem. Soc.* **2013**, *135*, 409.
[19] D. Cao, Z. Liu, P. Verwilst, S. Koo, P. Jangjili, J. S. Kim, W. Lin, *Chem. Rev.* **2019**, *119*, 10403.
[20] S.-K. Ko, Y.-K. Yang, J. Tae, I. Shin, *J. Am. Chem. Soc.* **2006**, *128*, 14150.
[21] L. Zhao, W. Li, A. Plog, Y. Xu, G. Buntkowsky, T. Gutmann, K. Zhang, *Phys. Chem. Chem. Phys.* **2014**, *16*, 26322.
[22] M. A. Khan, M. R. Siddiqui, M. Otero, S. A. Alshareef, M. Rafatullah, *Polymer* **2020**, *12*, 500.
[23] S. L. Levit, R. C. Walker, C. Tang, *Polymer* **2019**, *11*, 1406.
[24] S. Tommasone, F. Allabush, Y. K. Tagger, J. Norman, M. Köpf, J. H. Tucker, P. M. Mendes, *Chem. Soc. Rev.* **2019**, *48*, 5488.
[25] S. A. Asher, V. L. Alexeev, A. V. Goponenko, A. C. Sharma, I. K. Lednev, C. S. Wilcox, D. N. Finegold, *J. Am. Chem. Soc.* **2003**, *125*, 3322.
[26] R. Nishiyabu, Y. Kubo, T. D. James, J. S. Fossey, *Chem. Commun.* **2011**, *47*, 1106.
[27] Z. Li, L. Sun, Y. Zhang, A. P. Dove, R. K. O'Reilly, G. Chen, *ACS Macro Lett.* **2016**, *5*, 1059.
[28] Z. Cai, A. Sasmal, X. Liu, S. A. Asher, *ACS Sens.* **2017**, *2*, 1474.
[29] N. Jiang, Q. Huang, J. Liu, N. Liang, Q. Li, Q. Li, S.-S. Xie, *Eur. J. Med. Chem.* **2018**, *146*, 287.
[30] W. Li, W. Wang, Y. Yang, K. Zhang, *J. Mater. Chem. A* **2014**, *2*, 13675.
[31] K. Zhang, A. Geissler, T. Heinze, *Part. Part. Syst. Charact.* **2015**, *32*, 258.

SUPPORTING INFORMATION

Additional supporting information may be found online in the Supporting Information section at the end of this article.

How to cite this article: Wang S, Vana P, Zhang K. Mannosylated fluorescent cellulose-based glycopolymers for stable uniform nanoparticles. *J Polym Sci*. 2021;59:170–181. https://doi.org/10.1002/pol.20200714